ACS APPLIED MATERIALS & INTERFACES

Research Article

www.acsami.org

Thermally Stable Cellulose Nanocrystals toward High-Performance 2D and 3D Nanostructures

Chao Jia,[†,‡,§] Huiyang Bian,[§] Tingting Gao,[†] Feng Jiang,[†] Iain Michael Kierzewski,[†] Yilin Wang,[†] Yonggang Yao,[†] Liheng Chen,[§] Ziqiang Shao,[‡] J. Y. Zhu,[*,§] and Liangbing Hu[*,†]

[†]Department of Materials Science and Engineering, University of Maryland College Park, College Park, Maryland 20742, United States

[‡]School of Materials Science and Engineering, Beijing Institute of Technology, Beijing 100081, China

[§]Forest Products Laboratory, USDA Forest Service, Madison, Wisconsin 53726, United States

Supporting Information

ABSTRACT: Cellulose nanomaterials have attracted much attention in a broad range of fields such as flexible electronics, tissue engineering, and 3D printing for their excellent mechanical strength and intriguing optical properties. Economic, sustainable, and eco-friendly production of cellulose nanomaterials with high thermal stability, however, remains a tremendous challenge. Here versatile cellulose nanocrystals (DM-OA-CNCs) are prepared through fully recyclable oxalic acid (OA) hydrolysis along with disk-milling (DM) pretreatment of bleached kraft eucalyptus pulp. Compared with the commonly used cellulose nanocrystals from sulfuric acid hydrolysis, DM-OA-CNCs show several advantages including large aspect ratio, carboxylated surface, and excellent thermal stability along with high yield. We also successfully demonstrate the fabrication of high-performance films and 3D-printed patterns using DM-OA-CNCs. The high-performance films with high transparency, ultralow haze, and excellent thermal stability have the great potential for applications in flexible electronic devices. The 3D-printed patterns with porous structures can be potentially applied in the field of tissue engineering as scaffolds.

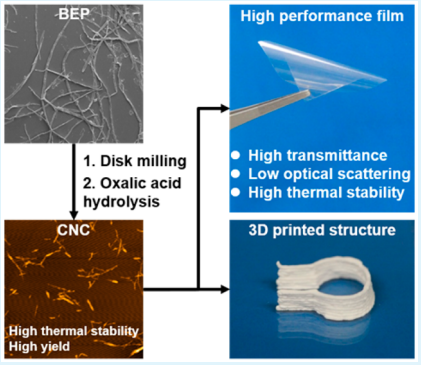

KEYWORDS: *cellulose nanocrystals, transparent film, 3D printing, high thermal stability, flexible electronics*

INTRODUCTION

Flexible transparent substrates have been ubiquitously used in a wide variety of fields including display electronics,[1,2] touch screens,[3,4] flexible transistors,[5,6] and photovoltaics.[7,8] Plastics are the most commonly used flexible substrate materials. However, they suffer from nonbiodegradability, high coefficient of thermal expansion, low thermal durability, and high processing temperature. Compared with plastics, nanopaper made of cellulose nanomaterials has merits in terms of environmental friendliness, flexibility, optical transparency, and printability.[9,10] Usually, cellulose nanomaterials are prepared by chemical modification methods such as TEMPO-mediated oxidation[11,12] and concentrated mineral acid hydrolysis,[13−15] resulting in low thermal durability[16,17] that limits their applications in flexible electronic devices due to the high processing temperature up to 150 °C.[18,19] Thus, developing thermal stable cellulose nanomaterials is urgent for flexible electronics applications.

3D printing, another technology, has attracted extensive attention in both industry and academia in recent years. Various objects and patterns can be obtained rapidly and economically by 3D printing. The 3D-printed structures have wide applications, such as tissue engineering,[20] energy storage,[21] microfluidic devices,[22] high-temperature heater,[23] and so on. The proper printing materials or "inks" are crucial to reliable 3D printing, which should possess high viscosity and shear-thinning behavior. The most common 3D printing materials are metals and polymers, but they need to be melted at high temperature. Substantial efforts have been dedicated to searching for hydrogel inks from biobased materials. Cellulose nanomaterials are attractive as ink for 3D printing because of their abundance, renewability, and nonpolluting characteristics.[24,25] In addition, demand for cellulose nanomaterials is increasing in many other application fields. It is worthy to note that biocompatible microcontainers have been demonstrated using cellulose nanocrystals (CNCs) as the shell,[26,27] and the CNCs shell of these microcontainers may be fully destroyed when exposed to external stimuli, such as ultrasound,[28] thus resulting in a controlled (multistage) release. Economic, sustainable, and eco-friendly production of cellulose nanomaterials, however, remains a tremendous challenge to realize these potentials.

To address the concerns of low thermal stability and high cost of existing cellulose nanomaterials for applications in

Received: June 17, 2017
Accepted: August 2, 2017
Published: August 2, 2017

DOI: 10.1021/acsami.7b08760
ACS Appl. Mater. Interfaces 2017, 9, 28922−28929

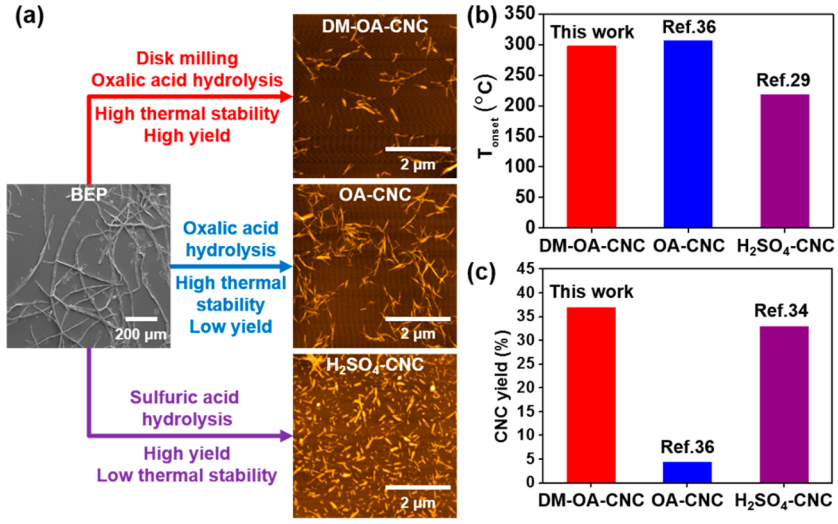

Figure 1. Comparison of CNC preparation processes. (a) Comparison of different CNC preparation processes. (b) T_{onset} comparison of CNCs prepared by different methods. (c) Comparison of CNC yield. Disk-milling pretreatment increases CNC yields 7-fold compared with that directly from oxalic acid hydrolysis.

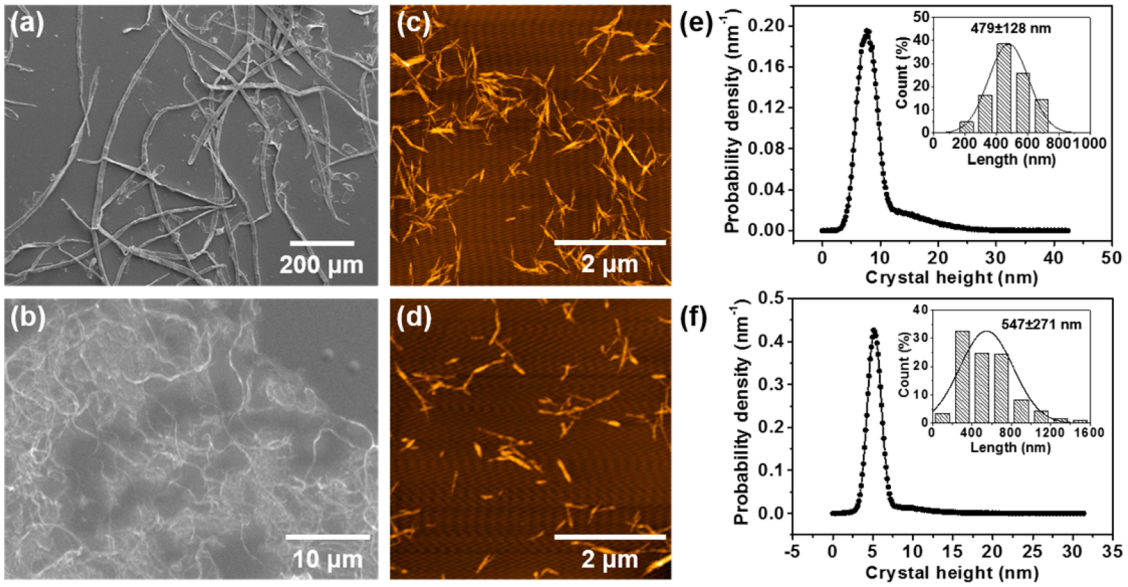

Figure 2. Morphology characterization of the raw materials and the resultant CNCs. (a) SEM image of the original BEP fibers. (b) SEM image of DM-BEP. Most BEP fibers were substantially fibrillated and shortened after disk-milling. AFM topographic images of (c) OA-CNCs and (d) DM-OA-CNCs. Length and height distributions of (e) OA-CNCs and (f) DM-OA-CNCs.

flexible electronics and 3D printing, here we demonstrate potentially low cost and environmentally sustainable production of cellulose nanocrystals (CNCs) using fully recyclable dicarboxylic acid (DCA) hydrolysis. DCA-CNC has good thermal stability as demonstrated previously.[29] However, the applicability of DCA-CNC for producing films with good mechanical strength for flexible electronics and inks with good rheological property for 3D printing has not been evaluated. We demonstrated that the longer crystal length or greater aspect ratio of DCA-CNC[29,30] compared with conventional mineral acid CNC[31] can address the poor mechanical property problem associated with mineral acid CNC films. Disk-milling pretreatment of pulp fibers was carried out before acid hydrolysis to improve cellulose accessibility and thereby CNC yield to reduce DCA-CNC cost. When using a DCA with a low solubility at ambient temperature, such as oxalic acid (OA), it can be easily recycled through a commercially proven crystallization technology.[29] With improved CNC yield through disk-milling pretreatment in the present study, along with good thermal stability and suitable rheological properties for 3D printing inks, DCA-CNC can be a commercially viable cellulose nanomaterial for flexible electronics and tissue engineering scaffolds through 3D printing.

■ RESULTS AND DISCUSSION

Different CNCs preparation processes were compared in Figure 1. The CNC yield of approximately 30% from sulfuric acid hydrolysis of pulp fibers (H_2SO_4−CNCs) was reported in the literature.[32−34] H_2SO_4−CNCs show poor thermal stability due to the existence of ester sulfate groups. The sulfate groups can dramatically reduce the thermal degradation temperature of H_2SO_4−CNCs because less energy is needed for the removal of

DOI: 10.1021/acsami.7b08760
ACS Appl. Mater. Interfaces 2017, 9, 28922−28929

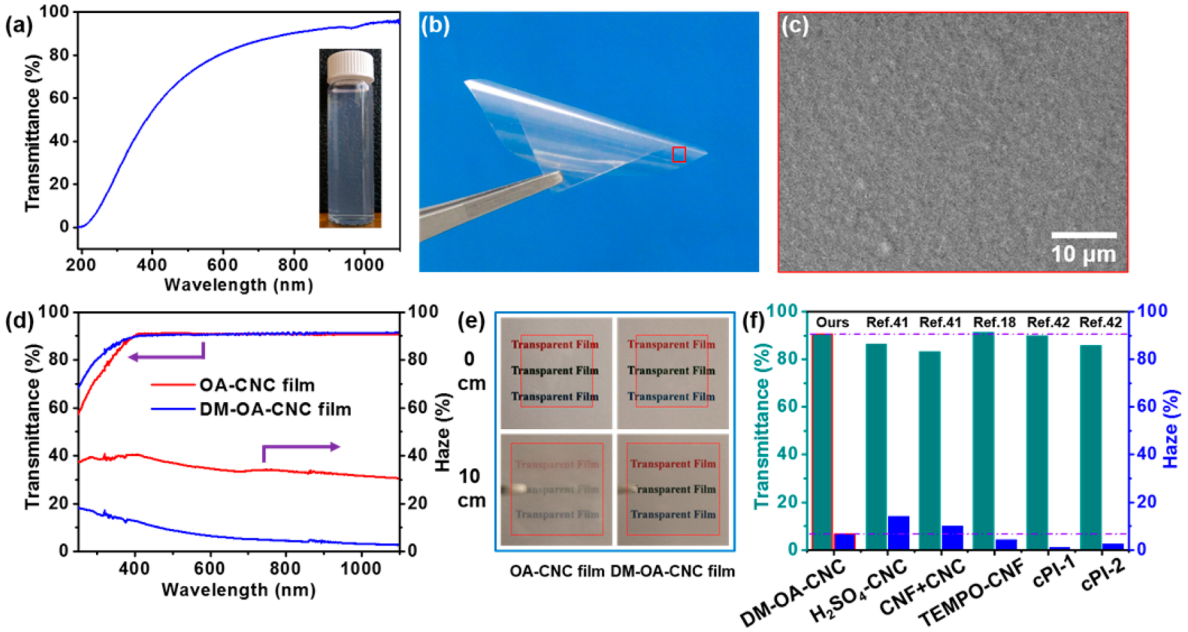

Figure 3. Optical properties of CNC suspension and films. (a) Transmittance spectra of DM-OA-CNC suspension. Inset is a photo of DM-OA-CNC suspension at 0.1 wt %. (b) A photograph of DM-OA-CNC film to show its flexibility. (c) SEM image of DM-OA-CNC film, indicating that the film has a flat surface. (d) The total transmittance and haze of OA-CNC film and DM-OA-CNC film. (e) OA-CNC film (left) and DM-OA-CNC film (right) were placed directly on the substrate with colored words (top panel) and 10 cm above the substrate (bottom panel). (f) Comparison of the total transmittance and haze between DM-OA-CNC film and other cellulose films and transparent polymer substrates at 600 nm wavelength.[18,41,42]

sulfate groups from the sulfated anhydroglucose units, and they can be removed at lower temperature as a result. In addition, the removed sulfuric acid molecules cannot be decomposed at low temperature (<380 °C), and they would catalyze the thermal decomposition of cellulose by removing some of the ring hydroxyl groups.[17,35] Therefore, the onset decomposition temperatures (T_{onset}) of H_2SO_4−CNCs is only 218 °C[29] (Figure 1b). Here the T_{onset} was defined as $dW/dT \geq -1$, i.e., at which the weight loss is higher than or equal to 1% with an increase of temperature by 1 °C.[29] Our previous research has indicated that the CNCs (named as OA-CNCs) prepared from direct oxalic acid (OA) hydrolysis of bleached eucalyptus pulp fibers (BEP) have high thermal stability with T_{onset} of up to 307 °C but low yield of only 4.4% at O50T100t60 (abbreviated for oxalic acid concentration of 50 wt % at 100 °C for 60 min).[36] Predisk-milling of BEP did not significantly reduce the thermal stability of the resultant CNCs (named as DM-OA-CNCs) with T_{onset} of 298 °C (Figure 1b), but substantially improved yield of 36.9% (Figure 1c). The CNC yield was improved over 7-fold with predisk-milling under the same OA hydrolysis condition. Such high CNC yield is comparable to the typical CNC yield from sulfuric acid hydrolysis in most reported studies.[32−34]

The original BEP fibers have a typical diameter of about 12 μm as shown in Figures 2a and S1. The compression force in disk-milling produced internal fiber delamination by breaking cross-links between fibrils, while shear and friction forces produced external fibrils from fiber surface, cut fibers, and increased the fiber external surface area[37,38] (Figures 2b, S2, and S3). The delaminated, fibrillated, and shortened fibers (DM-BEP) were hydrolyzed into CNCs (DM-OA-CNCs) using oxalic acid, as shown in Figures 2d and S4. Quantitative analyses of the AFM images indicate that the resultant DM-OA-CNCs have an average length of 547 nm and averaged height of 5 nm (Figure 2f), resulting in a large aspect ratio of 109. The cellulosic solid residue (CSR) after separating CNCs from hydrolyzed DM-BEP remains as partially hydrolyzed fibers (Figures S5−S7) with a yield of 52.5%. CSR can be used for cellulose nanofibrils (CNFs) production through subsequent mechanical nanofibrillation as we described previously.[29,30,34] We compared the morphology and size distributions of DM-OA-CNCs (Figures 2d,f and S4) with OA-CNCs (Figures 2c,e and S8). The OA-CNCs have a shorter average length of 479 nm and a greater average height of 8 nm, leading to an aspect ratio of 60, which is lower than that of DM-OA-CNCs.

The XRD patterns of BEP, DM-BEP, and the resultant CNCs were also obtained to determine the crystallinity index (CrI) values and crystallite dimensions. The XRD patterns have three characteristic peaks at about 16.4°, 22.6°, and 34.5° (Figure S9), corresponding to the (110), (200), and (004) reflection planes of typical cellulose I structure, respectively.[39] The calculated CrI of BEP is 77.3%. Disk-milling pretreatment substantially reduces the CrI value of DM-BEP to 70.7%. After OA hydrolysis, the CrI of DM-OA-CNCs increases to 78.5%, which can be attributed to the removal of noncellulosic polysaccharides and the dissolution of disordered cellulose regions.[35] Note that the crystallite dimensions of DM-OA-CNCs are 2.34 and 2.78 nm at (110) and (200) planes, respectively, which are similar to that of BEP raw material (2.21 (110) and 2.89 nm (200)) but higher than that of DM-BEP (2.07 (110) and 2.42 nm (200)).

Transmittance of the DM-OA-CNC suspension with 0.1 wt % concentration is very high, up to 81% at 600 nm wavelength (Figure 3a). The film made of DM-OA-CNCs has excellent flexibility (Figure 3b) because dicarboxylic acid produced CNC has long length of over 500 nm (Figure 2f), very different from films produced from standard sulfuric acid CNCs (~100 nm in length), which are very brittle. CNC film from sulfuric acid

DOI: 10.1021/acsami.7b08760
ACS Appl. Mater. Interfaces 2017, 9, 28922−28929

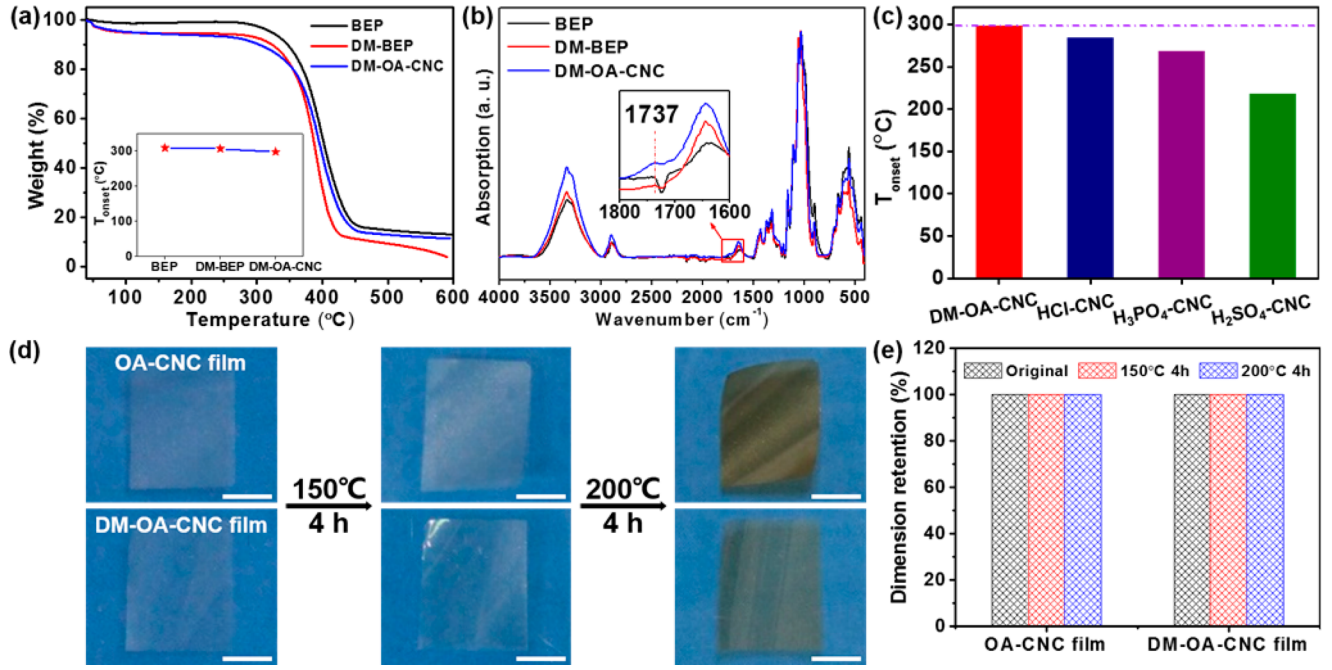

Figure 4. Thermal properties of CNCs and their films. (a) TG curves of BEP, DM-BEP and the corresponding DM-OA-CNCs. Inset shows the T_{onset} change. DM-OA-CNCs have the similar thermal stability as the raw materials. (b) FTIR spectra of BEP, DM-BEP, and DM-OA-CNCs. (c) T_{onset} comparison of CNCs prepared by different acid hydrolysis methods. (d) Comparison of thermal stability of OA-CNC film and DM-OA-CNC film in air. The scale bar is 5 mm. (e) Dimensional stability of OA-CNC film and DM-OA-CNC film. The dimension denotes the area of CNC films.

hydrolyzed CNCs is too brittle to conduct mechanical testing to obtain stress−strain curve data.[40] In comparison, OA-CNC and DM-OA-CNC films have excellent mechanical properties as shown in Figure S10. The OA-CNC film has a tensile strength of 24.56 MPa and an elongation at break of 0.55%. The DM-OA-CNC film shows an improved tensile strength of 31.75 MPa and elongation at break of 0.78%. The improved mechanical properties of the DM-OA-CNC film can be attributed to the large aspect ratio of DM-OA-CNCs. We also observed the top surface morphology of DM-OA-CNC film, showing a flat surface (Figure 3c), while OA-CNC film has a relatively rough surface (Figure S11).

The DM-OA-CNC film and OA-CNC film have similar light transmittance (Figure 3d). Their light transmittance is approximately 91% in the wavelength range of 400−1100 nm, or highly transparent. However, both CNC films have relatively low haze, especially the DM-OA-CNC film with a haze of merely 2.7% at 1100 nm. Figure 3e shows the OA-CNC film (left) and DM-OA-CNC film (right) were placed directly on the substrate with colored words (top panel) and 10 cm above the substrate (bottom panel). The similarity in transparency and difference in haze between the two films can be clearly seen (also see Figure S12). The blurred image suggests that the OA-CNC film has a higher haze than that of DM-OA-CNC film. In addition, the DM-OA-CNC film also demonstrates comparable optical performances with some other cellulose films and transparent polymer substrates[18,41,42] as shown in Figure 3f, so it has the potential to replace some traditional transparent materials in flexible electronic devices.

The thermal stability of cellulose nanomaterials is critical to their applications in electronic devices. The TG and DTG curves of BEP, DM-BEP, and DM-OA-CNCs were obtained, as shown in Figures 4a and S13. Slight weight loss is observed in the temperature range of 40−120 °C for all the samples owning to the evaporation of absorbed water. There is no noticeable weight loss during the range of 120−280 °C. Another thermal degradation process happens at about 280 °C, which can be ascribed to the decomposition of cellulose resulting from the destruction of hydrogen bonds. In this main thermal degradation process, cellulose was decomposed into tar, ash, and condensable and noncondensable gases by complicated transglycosidation and dehydration reactions.[43] The onset decomposition temperatures (T_{onset}) of BEP, DM-BEP and the resultant DM-OA-CNCs are 309, 307, and 298 °C, respectively. The reduction in thermal stability of DM-BEP and CNCs can be ascribed to the decreased dimension and increased surface area during disk-milling and oxalic acid hydrolysis, which enhances the exposure surface area to heat.[44]

The thermal stability of CNCs is also related to the characteristic and concentration of the surface chemical groups.[45] Typical absorption peaks of cellulosic material can be identified from the FTIR spectra of BEP, DM-BEP, and DM-OA-CNCs (Figure 4b and Table S2). Compared with that of BEP and DM-BEP, the FTIR spectrum of DM-OA-CNC has a new peak at around 1737 cm^{-1} (inset of Figure 4b) that can be attributed to the C═O ester vibrational stretching band.[46,47] This is indicative of esterification of cellulose by one of the carboxyl groups in oxalic acid.[29] We posit that only one of the carboxyl groups in oxalic acid esterified cellulose and that the other carboxyl group remained on CNCs surface; thus, the CNCs were carboxylated and charged. This is corroborated by conductometric titration that shows a content of carboxyl groups of 0.106 mmol/g CNC to result in a zeta potential value of −31.1 ± 1.8 mV. The existence of carboxyl groups on DM-OA-CNCs may also be a reason for the reduction in thermal stability. Even so, the DM-OA-CNCs remain highly thermal stable.

The T_{onset} of CNCs prepared by sulfuric, hydrochloric, and phosphoric acid hydrolysis are 218, 284, and 268 °C, respectively.[29] Compared with the CNCs prepared by mineral

DOI: 10.1021/acsami.7b08760
ACS Appl. Mater. Interfaces 2017, 9, 28922−28929

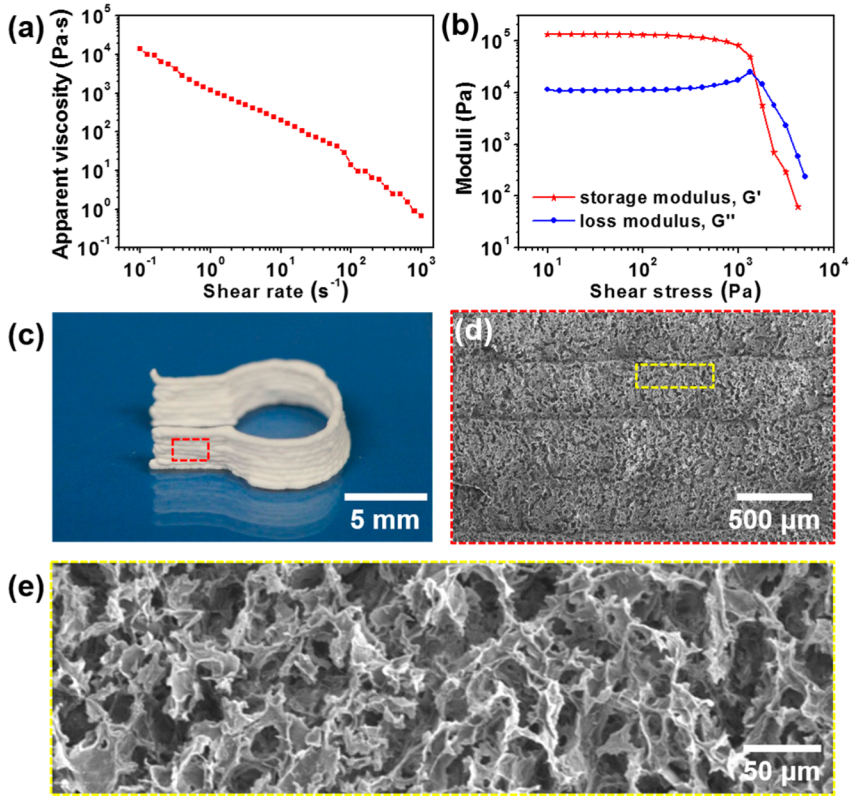

Figure 5. Rheological properties of DM-OA-CNC ink and 3D-printed pattern. (a) Apparent viscosity as a function of shear rate. (b) Storage and loss moduli as a function of shear stress. (c) Layer-by-layer 3D-printed pattern. (d) Surface morphology SEM image of 3D-printed pattern. (e) High-magnification SEM showing the surface morphology of 3D-printed pattern.

acid hydrolysis, DM-OA-CNCs from the same raw material exhibit higher thermal stability (Figure 4c). In addition, DM-OA-CNCs also show competitive thermal stability compared with CNCs from other cellulosic resources and preparation methods (Table S3). The thermal stability of the OA-CNC film and DM-OA-CNC film was also investigated by heating in air (Figure 4d). No visible changes in appearance were observed when the CNC films were heated at 150 °C for 4 h, suggesting their suitability for electronic device fabrication.[19] The CNC films became yellow when heated to 200 °C. The coloration of the DM-OA-CNC film is less pronounced compared with the OA-CNC film, indicating that the DM-OA-CNC film possesses better thermal stability as a result of the lower carboxyl group content of DM-OA-CNC than that of OA-CNC of 0.199 mmol/g CNC. In addition, both OA-CNC film and DM-OA-CNC film demonstrate excellent dimensional stability when heated at 150 and 200 °C for 4 h, respectively (Figure 4e), which is much better than some commonly used plastics.[48]

For the application of CNC film as substrate in flexible electronic devices, the electrical property is also important, so the electrical conductivities of OA-CNC film and DM-OA-CNC film were determined under this consideration. Note that the OA-CNC film and DM-OA-CNC film possess an electrical conductivity of 9.6×10^{-8} S/cm and 6.6×10^{-8} S/cm, respectively, indicating that the CNC films are insulating. The favorable insulating property, together with the excellent optical property and thermal stability will enable the CNC films to be applied in flexible electronic devices.

In addition to producing high-performance films, DM-OA-CNCs were also used for 3D printing. The rheological property of ink is most important in 3D printing and can affect 3D printing process and the stability of printed patterns.[23,49] The aqueous DM-OA-CNC suspension was first freeze-dried into powders, then mixed with DI water at a concentration of around 15 wt % to form DM-OA-CNC ink. The apparent viscosity of the DM-OA-CNC ink decreases linearly on the logarithmic scale with the increase in shear rate (Figure 5a), indicating that the ink is non-Newtonian fluid and exhibits shear-thinning behavior.[23] Storage modulus (G') shows a plateau value of about 10^5 Pa that exceeds the loss modulus (G'') by about 1 order of magnitude in the shear stress range of 10 Pa and 10^3 Pa (Figure 5b). The high G' shows that the DM-OA-CNC ink is stiff and has a solid-like nature in the quiescent state. At the crossing point between the two moduli curves, the shear yield stress is about 1500 Pa. The high stiffness and shear yield stress make the DM-OA-CNC ink suitable for 3D printing to result in layer-by-layer stacked structures with good shape stability. Some patterns have been successfully printed using DM-OA-CNCs as ink as shown in Figures 5c and S14. The structure of the printed patterns can be maintained by freeze-drying. SEM reveals the surface morphology of the 3D-printed pattern (Figures 5d and e). The layered structure consisting of stacked filaments with a width of ~300 μm can be observed (Figure 5d). In addition, porous structures generated by 3D printing using DM-OA-CNCs (Figure 5e) can be potentially applied in tissue engineering scaffolds due to the excellent biocompatibility.

CONCLUSIONS

Versatile cellulose nanocrystals with a high yield of 36.9% were prepared by fully recyclable oxalic acid hydrolysis and predisk-milling using bleached kraft eucalyptus pulp as the starting

DOI: 10.1021/acsami.7b08760
ACS Appl. Mater. Interfaces 2017, 9, 28922−28929

material. Rod-like DM-OA-CNCs with an average length of 547 nm and an average height of 5 nm were obtained, resulting in a large aspect ratio of 109. Compared with the CNCs prepared by mineral acid (sulfuric acid, hydrochloric acid, phosphoric acid) hydrolysis, the DM-OA-CNCs exhibit higher thermal stability with T_{onset} as high as 298 °C. We also successfully demonstrated the fabrication of high-performance films and 3D-printed patterns using DM-OA-CNCs. The prepared DM-OA-CNC film has very high transmittance and super low haze with respective values of 90.6% and 6.6% at the wavelength of 600 nm. In addition, the prepared film can be used at 150 °C for 4 h without discernible change in appearance, showing its suitability in electronic devices fabrication. Furthermore, the 3D-printed patterns with porous structures can be potentially applied in tissue engineering scaffolds due to the excellent biocompatibility of DM-OA-CNCs.

EXPERIMENTAL SECTION

Materials. Anhydrous oxalic acid (98%) was purchased from Sigma-Aldrich (St. Louis, MO). Bleached kraft eucalyptus dry lap pulp (BEP) was obtained from a commercial source (Fibria, Aracruz Cellulose, Brazil). The chemical composition of BEP was listed in Table S1. The AFM tips (Material: Si, N-type, 0.01−0.025 ohm/cm; Cantilever - L: 225 μm, W: 40 μm, T: 7.8 μm; Tip - Radius: < 10 nm, H: 14−16 μm; Resonance frequency: 160−225 kHz, Spring constant: 36−90 N/m; Coating: Al (Reflex side)) were purchased from Applied NanoStructures, Inc.

Disk-milling Pretreatment of BEP Fibers. The disk-milling pretreatment was proceeded according to the previous study.[50] BEP raw material was first soaked in deionized (DI) water for 12 h and then disintegrated at the rate of 3120 rpm for 10 000 revolutions using a laboratory disintegrator (Model 73−06−01, TMI, Ronkonkoma, New York, U.S.A.) to obtain the pulp suspension with a solid content of about 2% (w/w). After that, the BEP suspension was disk milled by a stone disk grinder SuperMassColloider (SMC) (model: MKZA6-2, disk model: MKGA6-80#, Masuko Sangyo Co., Ltd., Japan) at a rotation speed of 1500 rpm. The BEP suspension was pumped into the disk chamber under gravity from the hopper using a peristaltic pump (Cole Parmer, Chicago, IL, U.S.A.), and the fibrillated pulp suspension was obtained. The disk-milling time was 1 h. The disk-milled BEP was named as DM-BEP.

Oxalic Acid Hydrolysis Experiment. The oxalic acid hydrolysis experiment was carried out according to our previous study.[36] Oxalic acid concentration was 50 wt %, the reaction temperature was 100 °C, and the hydrolysis time was 1 h.

Preparation of CNC Films. CNC suspension (10 mL) with a concentration of 0.5 wt % was sonicated for 10 min for the uniform dispersion of CNCs. CNC films were prepared by casting the CNC suspension in plastic Petri dish, followed by air drying at room temperature to result in a film with a thickness of approximately 10 μm.

3D Printing Process. 3D printing was performed using a F4200N robot (Fisnar, NJ, U.S.A.). The printing nozzle diameter was approximately 300 μm. The printing pressure was 50 psi, the drop distance was 0.5 mm, and the moving speed of the nozzle was 5 mm/s. After printing, the printed pattern structures were freeze-dried at −51 °C with a vacuum pressure of 8 Pa to remove water and maintain the 3D structures.

CHARACTERIZATIONS

CNC yields were determined by a chemical oxygen demand (COD) method described previously.[34] The morphologies of the samples were obtained using a Zeiss EVO 40 SEM system (Carl Zeiss NTS, Peabody, MA). The morphologies of CNCs were observed by an AFM system (CS-3230, AFMWorkshop, CA, U.S.A.). The dimensions of the CNCs were obtained from the AFM images with a resolution of 512 pixels × 512 pixels without tip deconvolution. Zeta potential of CNC was measured using CNC suspension with a concentration of 0.2 g/L by a NanoBrook Omni Particle Size and Zeta Potential Analyzer (Brookhaven Instruments, Holtsville, NY, U.S.A.) based on phase analysis light scattering (PALS). FTIR spectra were recorded by a Fourier transform infrared (FTIR) spectroscopy system (Spectrum Two, PerkinElmer, Waltham, MA) with a universal attenuated-total-reflection (ATR) probe. The carboxyl group contents of CNC samples were determined by conductometric titration as described previously.[29,51] UV−vis light transmittance spectra of DM-OA-CNC suspension (0.1 wt %) was measured in a wavelength range of 190−1100 nm using a spectrophotometer (Model 8453, Agilent Technologies, Inc., U.S.A.). X-ray diffraction patterns of the samples were recorded on a X-ray diffractometer (Bruker D8 Discover, Bruker Co., Billerica, MA). The crystallinity index (CrI) was calculated according to a literature method without background subtraction.[52] The crystalline dimensions at different planes were calculated according to the Scherrer equation.[39] The thermal properties were measured using a thermogravimetric analyzer (Pyris 1 TGA, PerkinElmer Inc., Waltham, MA). The thermal stability of CNC films was evaluated by heating in a muffle furnace (Thermo Scientific, U.S.A.). The light transmittance spectrum and haze of the CNC films were determined using a UV−vis spectrophotometer with an integrated sphere (Lambda 35, PerkinElmer, U.S.A.). The mechanical strain−stress curves of the CNC films were determined by a dynamic mechanical analyzer (DMA Q800, TA Instruments). The electrical conductivity was determined by a four-point collinear probe method. The rheological property of DM-OA-CNC ink was measured by a stress-controlled rheometer (AR 2000, TA Instruments).

ASSOCIATED CONTENT

Supporting Information

The Supporting Information is available free of charge on the ACS Publications website at DOI: 10.1021/acsami.7b08760.

Chemical composition and diameter distribution of BEP; SEM images of DM-BEP, DM-BEP-CSR, and CNC film; AFM images of CNCs; XRD patterns and DTG curves of BEP, DM-BEP, and DM-OA-CNCs; mechanical properties of CNC films; digital images of CNC films and 3D-printed patterns; identifications of FTIR absorption peaks; and T_{onset} comparison of CNCs (PDF)

AUTHOR INFORMATION

Corresponding Authors

*E-mail: binghu@umd.edu.
*E-mail: jzhu@fs.fed.us.

ORCID

Ziqiang Shao: 0000-0002-8461-4979
J. Y. Zhu: 0000-0002-5136-0845
Liangbing Hu: 0000-0002-9456-9315

Author Contributions

L.H., J.Z., and C.J. designed the experiments. C.J. performed the fabrication processes of CNCs and the films. C.J. and I.K. carried out the optical property determination and thermal stability experiment of CNC films. C.J. and L.C. did the AFM

DOI: 10.1021/acsami.7b08760
ACS Appl. Mater. Interfaces 2017, 9, 28922−28929

characterization. H.B. determined the TGA, FTIR, and XRD characterizations. Y.W. measured the conductivity. Y.Y. and F.J. did the SEM characterization. T.G. did the mechanical test, rheological test, and 3D printing. All authors contributed to the manuscript writing.

Notes

The authors declare no competing financial interest.

■ ACKNOWLEDGMENTS

C.J. would like to thank the China Scholarship Council (CSC) for its financial support. The authors also acknowledge Brady Zarket for the rheological measurements.

■ REFERENCES

(1) Zhang, J.; Wang, C.; Zhou, C. Rigid/Flexible Transparent Electronics Based on Separated Carbon Nanotube Thin-Film Transistors and Their Application in Display Electronics. *ACS Nano* **2012**, *6*, 7412−7419.

(2) Chen, Y.; Au, J.; Kazlas, P.; Ritenour, A.; Gates, H.; McCreary, M. Electronic Paper: Flexible Active-matrix Electronic Ink Display. *Nature* **2003**, *423*, 136.

(3) Wang, J.; Liang, M.; Fang, Y.; Qiu, T.; Zhang, J.; Zhi, L. Rod-coating: towards Large-area Fabrication of Uniform Reduced Graphene Oxide Films for Flexible Touch Screens. *Adv. Mater.* **2012**, *24*, 2874−2878.

(4) Zhu, H.; Fang, Z.; Wang, Z.; Dai, J.; Yao, Y.; Shen, F.; Preston, C.; Wu, W.; Peng, P.; Jang, N.; Yu, Q.; Yu, Z.; Hu, L. Extreme Light Management in Mesoporous Wood Cellulose Paper for Optoelectronics. *ACS Nano* **2016**, *10*, 1369−1377.

(5) Fujisaki, Y.; Koga, H.; Nakajima, Y.; Nakata, M.; Tsuji, H.; Yamamoto, T.; Kurita, T.; Nogi, M.; Shimidzu, N. Transparent Nanopaper-Based Flexible Organic Thin-Film Transistor Array. *Adv. Funct. Mater.* **2014**, *24*, 1657−1663.

(6) Gaspar, D.; Fernandes, S. N.; de Oliveira, A. G.; Fernandes, J. G.; Grey, P.; Pontes, R. V.; Pereira, L.; Martins, R.; Godinho, M. H.; Fortunato, E. Nanocrystalline Cellulose Applied Simultaneously as the Gate Dielectric and the Substrate in Flexible Field Effect Transistors. *Nanotechnology* **2014**, *25*, 094008.

(7) Yin, Z.; Sun, S.; Salim, T.; Wu, S.; Huang, X.; He, Q.; Lam, Y. M.; Zhang, H. Organic Photovoltaic Devices Using Highly Flexible Reduced Graphene Oxide Films as Transparent Electrodes. *ACS Nano* **2010**, *4*, 5263−5268.

(8) Fan, Z.; Razavi, H.; Do, J.-w.; Moriwaki, A.; Ergen, O.; Chueh, Y.-L.; Leu, P. W.; Ho, J. C.; Takahashi, T.; Reichertz, L. A.; Neale, S.; Yu, K.; Wu, M.; Ager, J. W.; Javey, A. Three-dimensional Nanopillar-array Photovoltaics on Low-cost and Flexible Substrates. *Nat. Mater.* **2009**, *8*, 648−653.

(9) Jung, Y. H.; Chang, T. H.; Zhang, H.; Yao, C.; Zheng, Q.; Yang, V. W.; Mi, H.; Kim, M.; Cho, S. J.; Park, D. W.; Jiang, H.; Lee, J.; Qiu, Y.; Zhou, W.; Cai, Z.; Gong, S.; Ma, Z. High-performance Green Flexible Electronics Based on Biodegradable Cellulose Nanofibril Paper. *Nat. Commun.* **2015**, *6*, 7170.

(10) Li, Q.; Chen, W.; Li, Y.; Guo, X.; Song, S.; Wang, Q.; Liu, Y.; Li, J.; Yu, H.; Zeng, J. Comparative Study of the Structure, Mechanical and Thermomechanical Properties of Cellulose Nanopapers with Different Thickness. *Cellulose* **2016**, *23*, 1375−1382.

(11) Saito, T.; Hirota, M.; Tamura, N.; Kimura, S.; Fukuzumi, H.; Heux, L.; Isogai, A. Individualization of Nano-Sized Plant Cellulose Fibrils by Direct Surface Carboxylation Using TEMPO Catalyst under Neutral Conditions. *Biomacromolecules* **2009**, *10*, 1992−1996.

(12) Chen, W.; Li, Q.; Wang, Y.; Yi, X.; Zeng, J.; Yu, H.; Liu, Y.; Li, J. Comparative Study of Aerogels Obtained from Differently Prepared Nanocellulose Fibers. *ChemSusChem* **2014**, *7*, 154−161.

(13) Reid, M. S.; Villalobos, M.; Cranston, E. D. Benchmarking Cellulose Nanocrystals: From the Laboratory to Industrial Production. *Langmuir* **2017**, *33*, 1583−1598.

(14) Zoppe, J. O.; Peresin, M. S.; Habibi, Y.; Venditti, R. A.; Rojas, O. J. Reinforcing Poly(epsilon-caprolactone) Nanofibers with Cellulose Nanocrystals. *ACS Appl. Mater. Interfaces* **2009**, *1*, 1996−2004.

(15) Reid, M. S.; Villalobos, M.; Cranston, E. D. Cellulose Nanocrystal Interactions Probed by Thin Film Swelling to Predict Dispersibility. *Nanoscale* **2016**, *8*, 12247−12257.

(16) Fukuzumi, H.; Saito, T.; Okita, Y.; Isogai, A. Thermal Stabilization of TEMPO-oxidized Cellulose. *Polym. Degrad. Stab.* **2010**, *95*, 1502−1508.

(17) Roman, M.; Winter, W. T. Effect of Sulfate Groups from Sulfuric Acid Hydrolysis on the Thermal Degradation Behavior of Bacterial Cellulose. *Biomacromolecules* **2004**, *5*, 1671−1677.

(18) Yagyu, H.; Saito, T.; Isogai, A.; Koga, H.; Nogi, M. Chemical Modification of Cellulose Nanofibers for the Production of Highly Thermal Resistant and Optically Transparent Nanopaper for Paper Devices. *ACS Appl. Mater. Interfaces* **2015**, *7*, 22012−22017.

(19) Nogi, M.; Kim, C.; Sugahara, T.; Inui, T.; Takahashi, T.; Suganuma, K. High Thermal Stability of Optical Transparency in Cellulose Nanofiber Paper. *Appl. Phys. Lett.* **2013**, *102*, 181911.

(20) Malda, J.; Visser, J.; Melchels, F. P.; Jungst, T.; Hennink, W. E.; Dhert, W. J.; Groll, J.; Hutmacher, D. W. 25th Anniversary Article: Engineering Hydrogels for Biofabrication. *Adv. Mater.* **2013**, *25*, 5011−5028.

(21) Fu, K.; Yao, Y.; Dai, J.; Hu, L. Progress in 3D Printing of Carbon Materials for Energy-Related Applications. *Adv. Mater.* **2017**, *29*, 1603486.

(22) Duarte, L. C.; Colletes de Carvalho, T.; Lobo-Júnior, E. O.; Abdelnur, P. V.; Vaz, B. G.; Coltro, W. K. T. 3D Printing of Microfluidic Devices for Paper-assisted Direct Spray Ionization Mass Spectrometry. *Anal. Methods* **2016**, *8*, 496−503.

(23) Yao, Y.; Fu, K. K.; Yan, C.; Dai, J.; Chen, Y.; Wang, Y.; Zhang, B.; Hitz, E.; Hu, L. Three-Dimensional Printable High-Temperature and High-Rate Heaters. *ACS Nano* **2016**, *10*, 5272−5279.

(24) Håkansson, K. M. O.; Henriksson, I. C.; de la Peña Vázquez, C.; Kuzmenko, V.; Markstedt, K.; Enoksson, P.; Gatenholm, P. Solidification of 3D Printed Nanofibril Hydrogels into Functional 3D Cellulose Structures. *Advanced Materials Technologies* **2016**, *1*, 1600096.

(25) Siqueira, G.; Kokkinis, D.; Libanori, R.; Hausmann, M. K.; Gladman, A. S.; Neels, A.; Tingaut, P.; Zimmermann, T.; Lewis, J. A.; Studart, A. R. Cellulose Nanocrystal Inks for 3D Printing of Textured Cellular Architectures. *Adv. Funct. Mater.* **2017**, *27*, 1604619.

(26) Ye, C. H.; Malak, S. T.; Hu, K.; Wu, W.; Tsukruk, V. V. Cellulose Nanocrystal Microcapsules as Tunable Cages for Nano- and Micro particles. *ACS Nano* **2015**, *9*, 10887−10895.

(27) Kedzior, S. A.; Marway, H. S.; Cranston, E. D. Tailoring Cellulose Nanocrystal and Surfactant Behavior in Miniemulsion Polymerization. *Macromolecules* **2017**, *50*, 2645−2655.

(28) Korolovych, V. F.; Grishina, O. A.; Inozemtseva, O. A.; Selifonov, A. V.; Bratashov, D. N.; Suchkov, S. G.; Bulavin, L. A.; Glukhova, O. E.; Sukhorukov, G. B.; Gorin, D. A. Impact of High-frequency Ultrasound on Nanocomposite Microcapsules: in Silico and in Situ Visualization. *Phys. Chem. Chem. Phys.* **2016**, *18*, 2389−2397.

(29) Chen, L.; Zhu, J. Y.; Baez, C.; Kitin, P.; Elder, T. Highly Thermal-stable and Functional Cellulose Nanocrystals and Nanofibrils Produced Using Fully Recyclable Organic Acids. *Green Chem.* **2016**, *18*, 3835−3843.

(30) Wang, R.; Chen, L.; Zhu, J. Y.; Yang, R. Tailored and Integrated Production of Carboxylated Cellulose Nanocrystals (CNC) with Nanofibrils (CNF) through Maleic Acid Hydrolysis. *ChemNanoMat* **2017**, *3*, 328−335.

(31) Chen, L.; Wang, Q.; Hirth, K.; Baez, C.; Agarwal, U. P.; Zhu, J. Y. Tailoring the Yield and Characteristics of Wood Cellulose Nanocrystals (CNC) Using Concentrated Acid Hydrolysis. *Cellulose* **2015**, *22*, 1753−1762.

(32) Hamad, W. Y.; Hu, T. Q. Structure-Process-Yield Interrelations in Nanocrystalline Cellulose Extraction. *Can. J. Chem. Eng.* **2010**, *88*, 392−402.

DOI: 10.1021/acsami.7b08760
ACS Appl. Mater. Interfaces 2017, 9, 28922−28929

(33) Bondeson, D.; Mathew, A.; Oksman, K. Optimization of the Isolation of Nanocrystals from Microcrystalline Cellulose by Acid Hydrolysis. *Cellulose* **2006**, *13*, 171−180.
(34) Wang, Q. Q.; Zhu, J. Y.; Reiner, R. S.; Verrill, S. P.; Baxa, U.; McNeil, S. E. Approaching Zero Cellulose Loss in Cellulose Nanocrystal (CNC) Production: Recovery and Characterization of Cellulosic Solid Residues (CSR) and CNC. *Cellulose* **2012**, *19*, 2033−2047.
(35) Yu, H.; Qin, Z.; Liang, B.; Liu, N.; Zhou, Z.; Chen, L. Facile Extraction of Thermally Stable Cellulose Nanocrystals with a High Yield of 93% through Hydrochloric Acid Hydrolysis under Hydrothermal Conditions. *J. Mater. Chem. A* **2013**, *1*, 3938−3944.
(36) Jia, C.; Chen, L.; Shao, Z.; Agarwal, U. P.; Hu, L.; Zhu, J. Y. Using a Fully Recyclable Dicarboxylic Acid for Producing Dispersible and Thermally Stable Cellulose Nanomaterials from Different Cellulosic Sources. *Cellulose* **2017**, *24*, 2483−2498.
(37) Wang, Q. Q.; Zhu, J. Y.; Gleisner, R.; Kuster, T. A.; Baxa, U.; McNeil, S. E. Morphological Development of Cellulose Fibrils of a Bleached Eucalyptus Pulp by Mechanical Fibrillation. *Cellulose* **2012**, *19*, 1631−1643.
(38) Hu, C.; Zhao, Y.; Li, K.; Zhu, J. Y.; Gleisner, R. Optimizing Cellulose Fibrillation for the Production of Cellulose Nanofibrils by a Disk Grinder. *Holzforschung* **2015**, *69*, 993−1000.
(39) Lin, N.; Dufresne, A. Surface Chemistry, Morphological Analysis and Properties of Cellulose Nanocrystals with Gradiented Sulfation Degrees. *Nanoscale* **2014**, *6*, 5384−5393.
(40) Guidetti, G.; Atifi, S.; Vignolini, S.; Hamad, W. Y. Flexible Photonic Cellulose Nanocrystal Films. *Adv. Mater.* **2016**, *28*, 10042−10047.
(41) Xu, X.; Zhou, J.; Jiang, L.; Lubineau, G.; Ng, T.; Ooi, B. S.; Liao, H. Y.; Shen, C.; Chen, L.; Zhu, J. Y. Highly Transparent, Low-haze, Hybrid Cellulose Nanopaper as Electrodes for Flexible Electronics. *Nanoscale* **2016**, *8*, 12294−12306.
(42) Shen, J.; Li, F.; Cao, Z.; Barat, D.; Tu, G. Light Scattering in Nanoparticle Doped Transparent Polyimide Substrates. *ACS Appl. Mater. Interfaces* **2017**, *9*, 14990−14997.
(43) Borsoi, C.; Zimmernnam, M. V. G.; Zattera, A. J.; Santana, R. M. C.; Ferreira, C. A. Thermal Degradation Behavior of Cellulose Nanofibers and Nanowhiskers. *J. Therm. Anal. Calorim.* **2016**, *126*, 1867−1878.
(44) Lu, P.; Hsieh, Y.-L. Preparation and Properties of Cellulose Nanocrystals: Rods, Spheres, and Network. *Carbohydr. Polym.* **2010**, *82*, 329−336.
(45) Espinosa, S. C.; Kuhnt, T.; Foster, E. J.; Weder, C. Isolation of Thermally Stable Cellulose Nanocrystals by Phosphoric Acid Hydrolysis. *Biomacromolecules* **2013**, *14*, 1223−1230.
(46) Spinella, S.; Lo Re, G.; Liu, B.; Dorgan, J.; Habibi, Y.; Leclere, P.; Raquez, J.-M.; Dubois, P.; Gross, R. A. Polylactide/cellulose Nanocrystal Nanocomposites: Efficient Routes for Nanofiber Modification and Effects of Nanofiber Chemistry on PLA Reinforcement. *Polymer* **2015**, *65*, 9−17.
(47) Bian, H.; Chen, L.; Dai, H.; Zhu, J. Y. Integrated Production of Lignin Containing Cellulose Nanocrystals (LCNC) and Nanofibrils (LCNF) Using an Easily Recyclable Di-carboxylic Acid. *Carbohydr. Polym.* **2017**, *167*, 167−176.
(48) Li, L.; Yu, M.; Jia, C.; Liu, J.; Lv, Y.; Liu, Y.; Zhou, Y.; Liu, C.; Shao, Z. Cellulosic Biomass-Reinforced Polyvinylidene Fluoride Separators with Enhanced Dielectric Properties and Thermal Tolerance. *ACS Appl. Mater. Interfaces* **2017**, *9*, 20885−20894.
(49) Shepherd, J. N. H.; Parker, S. T.; Shepherd, R. F.; Gillette, M. U.; Lewis, J. A.; Nuzzo, R. G. 3D Microperiodic Hydrogel Scaffolds for Robust Neuronal Cultures. *Adv. Funct. Mater.* **2011**, *21*, 47−54.
(50) Qin, Y.; Qiu, X.; Zhu, J. Y. Understanding Longitudinal Wood Fiber Ultra-structure for Producing Cellulose Nanofibrils Using Disk Milling with Diluted Acid Prehydrolysis. *Sci. Rep.* **2016**, *6*, 35602.
(51) Bian, H.; Chen, L.; Wang, R.; Zhu, J. Green and Low-cost Production of Thermally Stable and Carboxylated Cellulose Nanocrystals and Nanofibrils Using Highly Recyclable Dicarboxylic Acids. *J. Visualized Exp.* **2017**, e55079.
(52) Segal, L.; Creely, J. J.; Martin, A. E.; Conrad, C. M. An Empirical Method for Estimating the Degree of Crystallinity of Native Cellulose Using the X-ray Diffractometer. *Text. Res. J.* **1959**, *29*, 786−794.

DOI: 10.1021/acsami.7b08760
ACS Appl. Mater. Interfaces 2017, 9, 28922−28929